

The transformed domain hybrid adaptive beamformer for multiple jammers suppression

Shiunn-Jang Chern, Chih-Yuan Sung and Kai-Ping Yang

Citation: *The Journal of the Acoustical Society of America* **95**, 866 (1994); doi: 10.1121/1.408397

View online: <https://doi.org/10.1121/1.408397>

View Table of Contents: <https://asa.scitation.org/toc/jas/95/2>

Published by the *Acoustical Society of America*

ARTICLES YOU MAY BE INTERESTED IN

[An approach for automatic classification of grouper vocalizations with passive acoustic monitoring](#)

The Journal of the Acoustical Society of America **143**, 666 (2018); <https://doi.org/10.1121/1.5022281>

[Statistics on noise covariance matrix for covariance fitting-based compressive sensing direction-of-arrival estimation algorithm: For use with optimization via regularization](#)

The Journal of the Acoustical Society of America **143**, 3883 (2018); <https://doi.org/10.1121/1.5042354>

[Ray-based blind deconvolution of shipping sources using multiple beams separated by alternating projection](#)

The Journal of the Acoustical Society of America **144**, 3525 (2018); <https://doi.org/10.1121/1.5083834>

[Mapping of ocean currents in shallow water using moving ship acoustic tomography](#)

The Journal of the Acoustical Society of America **145**, 858 (2019); <https://doi.org/10.1121/1.5090496>

[Observations of phase and intensity fluctuations for low-frequency, long-range transmissions in the Philippine Sea and comparisons to path-integral theory](#)

The Journal of the Acoustical Society of America **146**, 567 (2019); <https://doi.org/10.1121/1.5118252>

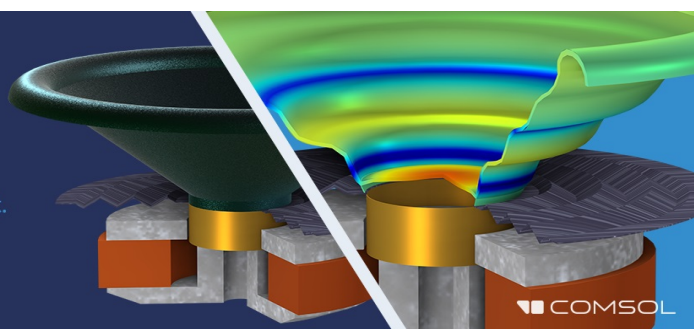
[Machine learning in acoustics: Theory and applications](#)

The Journal of the Acoustical Society of America **146**, 3590 (2019); <https://doi.org/10.1121/1.5133944>

Take the Lead in Acoustics

The ability to account for coupled physics phenomena lets you predict, optimize, and virtually test a design under real-world conditions – even before a first prototype is built.

» Learn more about **COMSOL Multiphysics®**



The transformed domain hybrid adaptive beamformer for multiple jammers suppression

Shiunn-Jang Chern and Chih-Yuan Sung

Institute of Electrical Engineering, National Sun Yat-Sen University, Kaohsiung, Taiwan 80424, Republic of China

Kai-Ping Yang

Communication Engineering Department, The National Kaohsiung Marine College, No. 142, Hai-Juan Road, Kaohsiung, Taiwan 811, Republic of China

(Received 13 April 1993; accepted for publication 11 October 1993)

The major area of current interest in adaptive arrays in their application to problems arising in radar, sonar, and communication systems, where the designer almost invariably faces the problem of interference suppression. In general, for real time processing, the robustness, with respect to the changed environment, of the adaptive beamforming algorithm with rapid convergence rate is desired. In this paper, a new hybrid adaptive beamforming algorithm is derived in the discrete-cosine transformed domain for multiple jammers suppression. Overall performance improvement, in terms of convergence rate and the computational requirement, is addressed. From computer simulation results, it was found that the presented method outperformed the conventional Frost's linear constraints LMS algorithm, in terms of the capability of jammers suppression and the rate of convergence.

PACS numbers: 43.60.Gk

INTRODUCTION

Adaptive array processing is now of growing importance in the field of communications, radar, sonar, and seismology systems, etc.^{1,2} The adaptive array can be used to achieve good nulling capability of the undesired interference adaptively over the conventional delay-and-sum beamforming array. Capon *et al.*³ invented linearly constrained adaptive beamforming in 1967. Griffiths and Jim⁴ advanced the generalized sidelobe canceler, which was equivalent to a Frost's beamformer under certain conditions.

It is well known that the performance of the conventional time domain LMS algorithm is highly related to the eigenvalue spread of the input autocorrelation matrix. Since the conventional Frost's linear constraints LMS⁵ (LCLMS), adaptive beamforming used the LMS algorithm during the adaptation processes. Similarly, the performance of the LCLMS beamforming algorithm may be very sensitive to the power ratio of the multiple jammers. Thus the LCLMS beamforming algorithm has some problems associated with performance degradation in the multiple jammers environment. To overcome this drawback, in this paper, a new hybrid linearly constrained LMS (HLCLMS) adaptive beamforming algorithm is proposed. The basic idea behind the new method is to use the transformed domain adaptive filtering technique along with the Frost's LCLMS algorithm to achieve the desired performance.

In this paper, we first develop the HLCLMS adaptive beamforming algorithm in the discrete cosine transformed domain and discusses the rationale behind it. Then the

attention is focused on the comparison with the conventional Frost's LCLMS adaptive beamforming algorithm in the multiple jammers environment. The robustness of the presented HLCLMS method with respect to the power ratio of the jammers is addressed.

I. REVIEW OF THE FROST'S LCLMS ALGORITHM

To proceed with the derivation of the hybrid adaptive beamforming algorithm in the transformed domain, we first review the conventional array system.⁵ In the conventional array system, a sampled-data version of the analog signal processor is considered in developing the optimum weight vector solution by assuming that the voltages appearing at each array tap are sampled every Δ seconds (Δ may be a multiple of the delay τ). The vector of sampled signals at the time index is denoted by $\mathbf{x}(n)$ and is defined by

$$\mathbf{x}(n) \equiv [x_1(n\Delta), x_2(n\Delta), \dots, x_{KL}(n\Delta)]^T. \quad (1)$$

The subscript KL denotes K times L , where K and L are the number of channels and tap delay lines, respectively. Any sampled signals that appear may be regarded as the sum of signals due to the look direction signals \mathbf{s} and non-look direction noises \mathbf{n} , so that

$$\mathbf{x}(n) = \mathbf{s}(n) + \mathbf{n}(n). \quad (2)$$

The vectors of the look signal and the nonlook direction noises are defined by

$$\mathbf{s}(n) \equiv [\underbrace{s(n\Delta), \dots, s(n\Delta)}_{K \text{ taps}}, \underbrace{s(n\Delta - \tau), \dots, s(n\Delta - \tau)}_{K \text{ taps}}, \dots, \underbrace{s(n\Delta - (L-1)\tau)}_{K \text{ taps}}]^T \quad (3a)$$

$K \times L$

and

$$\mathbf{n}(n) = [n_1(n\Delta), n_2(n\Delta), \dots, n_{KL}(n\Delta)]^T, \quad (3b)$$

respectively. The vector of weight appearing at each tap is denoted by $\mathbf{w}(n)$, where

$$\mathbf{w}(n) = [w_1(n), w_2(n), \dots, w_{KL}(n)]^T. \quad (4)$$

We assume that both the signals and noises can be modeled as zero-mean random processes with unknown second-order statistics. The covariance matrix of \mathbf{x} is designated as $\mathbf{R}_{\mathbf{xx}} = E\{\mathbf{x}(n)\mathbf{x}^T(n)\}$. The vector of look direction signals, $\mathbf{s}(n)$, is assumed to be uncorrelated with the vector of nonlook direction noises, $\mathbf{n}(n)$.

The expected value of the array output power is given by

$$E\{y^2(n)\} = E\{\mathbf{w}(n)^T \mathbf{x}(n) \mathbf{x}^T(n) \mathbf{w}(n)\} = \mathbf{w}^T \mathbf{R}_{\mathbf{xx}} \mathbf{w}. \quad (5)$$

Define a $KL \times L$ constraint matrix \mathbf{C} having \mathbf{c}_j by $\mathbf{C} = [\mathbf{c}_1, \dots, \mathbf{c}_j, \dots, \mathbf{c}_L]$ with \mathbf{c}_j , $j = 1, \dots, L$, being the $KL \times 1$ column vector. The entries of the j th group of K elements of \mathbf{c}_j are unity and zero otherwise. Furthermore we define the L -dimensional vector, $\mathbf{f} = [f_1, f_2, \dots, f_L]^T$, such that $\mathbf{C}^T \mathbf{w}(n) = \mathbf{f}$.

Since the look direction frequency response is fixed by the constraint described above, minimizing the total output power given by (5), the constrained optimization problem can be expressed as

$$\underset{\mathbf{w}}{\text{minimize}} \quad \mathbf{w}^T(n) \mathbf{R}_{\mathbf{xx}} \mathbf{w}(n), \quad (6)$$

$$\text{subject to} \quad \mathbf{C}^T \mathbf{w}(n) = \mathbf{f}. \quad (7)$$

Finding the optimal weight vector \mathbf{w}_{opt} to satisfy (6) and (7) can be accomplished by the method of Lagrange multiplier. From Ref. 6 we have

$$\mathbf{w}_{\text{opt}} = \mathbf{R}_{\mathbf{xx}}^{-1} \mathbf{C} [\mathbf{C}^T \mathbf{R}_{\mathbf{xx}}^{-1} \mathbf{C}]^{-1} \mathbf{f}, \quad (8)$$

where the existence of $[\mathbf{C}^T \mathbf{R}_{\mathbf{xx}}^{-1} \mathbf{C}]^{-1}$ is guaranteed by the fact that $\mathbf{R}_{\mathbf{xx}}$ is positive definite⁷ and \mathbf{C} has full rank.

For convenience, we define the KL -dimensional column vector as

$$\mathbf{g} \equiv \mathbf{C} (\mathbf{C}^T \mathbf{C})^{-1} \mathbf{f} \quad (9)$$

and the $KL \times KL$ matrix as

$$\mathbf{P} \equiv \mathbf{I} - \mathbf{C} (\mathbf{C}^T \mathbf{C})^{-1} \mathbf{C}^T, \quad (10)$$

where \mathbf{I} is the $KL \times KL$ identity matrix. Now, applying (9) and (10) to (8) and recognizing that $y(n) = \mathbf{x}^T(n) \mathbf{w}(n)$, the Frost's linear constrained LMS adaptive beamforming algorithm can be derived:⁵

$$\mathbf{w}(n+1) = \mathbf{P} [\mathbf{w}(n) - \mu y(n) \mathbf{x}(n)] + \mathbf{g}, \quad (11)$$

with the initial weight vector, $\mathbf{w}(0) = \mathbf{g}$ and the step size μ chosen to satisfy the condition⁵

$$0 < \mu < 2/3 \text{Tr}[\mathbf{R}_{\mathbf{xx}}] \quad (12)$$

to assure that the algorithm of (11) converges.

II. THE HYBRID ADAPTIVE BEAMFORMER

So far we have reviewed the conventional Frost's adaptive beamforming algorithm. In the following, we will apply the discrete cosine transform⁸ (DCT) to each sensor as depicted in Fig. 1. Based on the array structure shown in Fig. 1, the hybrid constrained adaptive beamforming algorithm can be derived. For convenience, we refer to the adaptive array of Fig. 1 as the transformed domain hybrid linear constraints LMS (HLCLMS) adaptive beamformer.

The HLCLMS adaptive beamformer depicted in Fig. 1 is implemented with K channels. In each channel, the tapped delay version of the received signals are first transformed by the DCT and then used in the HLCLMS adaptive beamforming algorithm for adaptation. For the i th channel, the vector of sampled signals at the n th time index

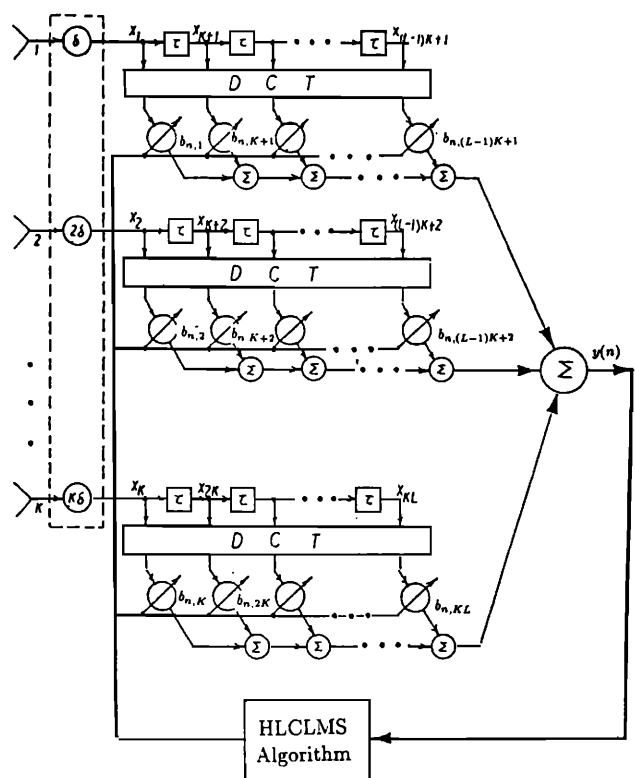


FIG. 1. The structure of the HLCLMS beamformer.

is denoted by $\mathbf{x}_i(n)$ and $\mathbf{z}_i(n)$ is the corresponding transformed signal vector. Both $\mathbf{x}_i(n)$ and $\mathbf{z}_i(n)$ are designated and related as

$$\mathbf{x}_i(n) = [x_i(n\Delta), x_{K+i}(n\Delta), \dots, x_{(L-1)K+i}(n\Delta)]^T, \quad i=1,2,\dots,K \quad (13)$$

and

$$\mathbf{z}_i(n) = \Phi^T \mathbf{x}_i(n) = [z_i(n\Delta), z_{K+i}(n\Delta), \dots, z_{(L-1)K+i}(n\Delta)]^T. \quad (14)$$

In (14), the DCT transformation matrix Φ^T is given by

$$\Phi^T \equiv \begin{bmatrix} \phi_{00} & \phi_{01} & \cdots & \phi_{0(L-1)} \\ \phi_{10} & \phi_{11} & \cdots & \phi_{1(L-1)} \\ \vdots & \vdots & \ddots & \vdots \\ \phi_{(L-1)0} & \phi_{(L-1)1} & \cdots & \phi_{(L-1)(L-1)} \end{bmatrix}, \quad (15)$$

with its entries being defined as⁸

$$\phi_{ij} = c_i \sqrt{\frac{2}{L}} \cos\left((2j+1) \frac{i\pi}{2L}\right), \quad i,j=0,1,\dots,L-1, \quad (16)$$

and

$$c_i = \begin{cases} \sqrt{\frac{1}{2}}, & i=0 \text{ or } L \\ 1, & i \neq 0. \end{cases}$$

Since

$$\sum_{m=0}^{L-1} \phi_{im} \phi_{jm} = \begin{cases} 1, & i=j, \\ 0, & i \neq j \end{cases}$$

we have that, $\Phi^T \Phi = \mathbf{I}_{L \times L}$ (i.e., Φ^T is an orthogonal matrix).

In the case that the size of tap weights is large, to save computation time and the consideration for hardware implementation, Chern⁹ derived a recursive DCT algorithm. For whole K channels, the KL -dimensional vector of sampled signals at the n th time index is denoted by $\mathbf{x}(n)$, i.e.,

$$\mathbf{x}(n) = [x_1(n\Delta), x_2(n\Delta), \dots, x_{KL}(n\Delta)]^T \quad (17)$$

and its corresponding transformed domain vector is represented by

$$\mathbf{z}(n) = \Psi^T \mathbf{x}(n) = [z_1(n\Delta), z_2(n\Delta), \dots, z_{KL}(n\Delta)]^T. \quad (18)$$

From (14), (15), and (18), it is clearly that the transformation matrix (Ψ^T) can be expressed as

$$\Psi^T = \begin{bmatrix} [\psi_{00}] & [\psi_{01}] & \cdots & [\psi_{0(L-1)}] \\ [\psi_{10}] & [\psi_{11}] & \cdots & [\psi_{1(L-1)}] \\ \vdots & \vdots & \ddots & \vdots \\ [\psi_{(L-1)0}] & [\psi_{(L-1)1}] & \cdots & [\psi_{(L-1)(L-1)}] \end{bmatrix}, \quad (19)$$

with

$$[\psi_{ij}] = \begin{bmatrix} \phi_{ij} & 0 & \cdots & 0 \\ 0 & \phi_{ij} & \cdots & 0 \\ \vdots & \vdots & \ddots & \vdots \\ 0 & 0 & \cdots & \phi_{ij} \end{bmatrix}_{K \times K}, \quad \text{for } i,j=0,1,\dots,L-1. \quad (20)$$

It is notice that based on the definition of (16), we can easily show that $\Psi^T \Psi = \mathbf{I}$. To derive the relationship between the Frost's LCLMS algorithm and the HLCLMS algorithm, we first premultiply Ψ^T on both sides of (11) yielding

$$\Psi^T \mathbf{w}(n+1) = \Psi^T \mathbf{P} [\mathbf{w}(n) - \mu \mathbf{y}(n) \mathbf{x}(n)] + \Psi^T \mathbf{g}. \quad (21)$$

Now let us define the corresponding transformed domain vectors of \mathbf{g} and $\mathbf{w}(n)$ as to be \mathbf{a} and $\mathbf{b}(n)$:

$$\mathbf{a} \equiv \Psi^T \mathbf{g} \quad (22)$$

and

$$\mathbf{b}(n) \equiv \Psi^T \mathbf{w}(n), \quad (23)$$

respectively, with $\mathbf{b}(n)$ being designated as

$$\mathbf{b}(n) = [b_{n,1}, b_{n,2}, \dots, b_{n,KL}]^T. \quad (24)$$

Using the definitions of (10) and (19), we can show that $\mathbf{P} = \Psi^T \mathbf{P} \Psi$ (see Appendix A). Now, using this fact and recognizing that $\mathbf{z}(n) = \Psi^T \mathbf{x}(n)$, (21) becomes

$$\begin{aligned} \mathbf{b}(n+1) &= \Psi^T \mathbf{w}(n+1) \\ &= \Psi^T \mathbf{P} \Psi [\mathbf{b}(n) - \mu \mathbf{y}(n) \Psi^T \mathbf{x}(n)] + \mathbf{a} \\ &= \mathbf{P} [\mathbf{b}(n) - \mu \mathbf{y}(n) \mathbf{z}(n)] + \mathbf{a}. \end{aligned} \quad (25)$$

From (8) and (23), the optimal transformed tap weight vector will be

$$\begin{aligned} \mathbf{b}_{\text{opt}} &= \Psi^T \mathbf{w}_{\text{opt}} \\ &= \Psi^T \mathbf{R}_{\mathbf{xx}}^{-1} \mathbf{C} [\mathbf{C}^T \mathbf{R}_{\mathbf{xx}}^{-1} \mathbf{C}]^{-1} \mathbf{f} \\ &= \mathbf{R}_{\mathbf{zz}}^{-1} (\Psi^T \mathbf{C}) [(\Psi^T \mathbf{C})^T \mathbf{R}_{\mathbf{zz}}^{-1} (\Psi^T \mathbf{C})]^{-1} \mathbf{f}, \end{aligned} \quad (26)$$

where $\mathbf{R}_{\mathbf{zz}}^{-1}$ is the inverse matrix of $\mathbf{R}_{\mathbf{zz}}$. Here, the transformed domain autocorrelation matrix $\mathbf{R}_{\mathbf{zz}}$ is defined as

$$\mathbf{R}_{\mathbf{zz}} = E\{\mathbf{z}(n) \mathbf{z}^T(n)\} = \Psi^T \mathbf{R}_{\mathbf{xx}} \Psi. \quad (27)$$

Similarly, the beamformer output of the transformed domain adaptive filter, by definition, is given by

$$y(n) = \mathbf{b}^T(n) \mathbf{z}(n) = \mathbf{w}^T(n) \Psi \Psi^T \mathbf{x}(n) = \mathbf{w}^T(n) \mathbf{x}(n). \quad (28)$$

From (28) we learn that the output signals of the transformed domain beamformer have a similar time domain expression as the Frost's LCLMS beamformer. Thus, in array processing, if the output signal is desired for further processing, the use of the transformed domain beamformer would not require any inverse transformation.

Moreover, the normalized power version of (25) can be similarly expressed by

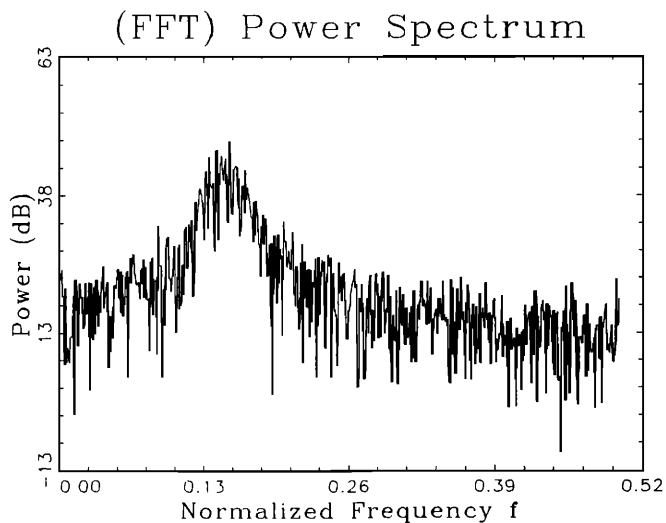


FIG. 2. The power spectrum of the look direction signal.

$$\mathbf{b}(n+1) = \mathbf{P}[\mathbf{b}(n) - \mathbf{U}y(n)\mathbf{z}(n)] + \mathbf{a} \quad (29)$$

with

$$\mathbf{U} = \text{diag}\{\mu(1), \mu(2), \dots, \mu(KL)\}, \quad (30)$$

where $\text{diag}\{\cdot\}$ denotes the diagonal matrix and the step size $\mu(i)$, $i=1, \dots, KL$, is given by

$$\mu(i) = \frac{\mu_s}{p_i(n\Delta)}, \quad (31)$$

where $p_i(n\Delta)$ is the averaged power of $z_i(n\Delta)$ and can only be estimated. In practice, for instance, we may use the following formula:

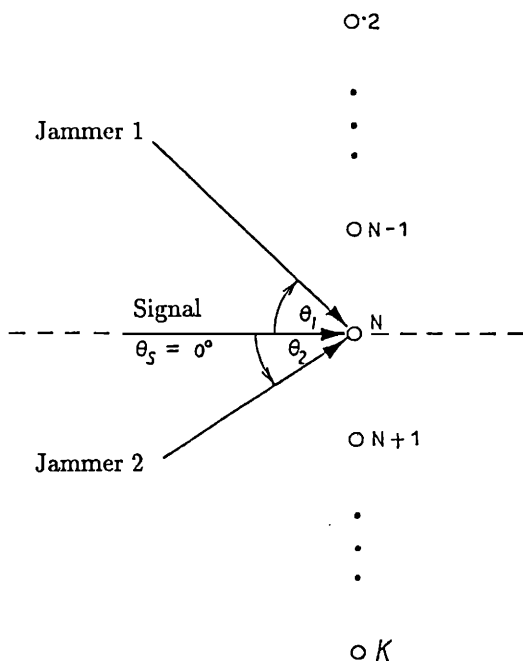


FIG. 3. Assumed signal and jammers distributions.

TABLE I. Case 1 jammers in simulation.

	Direction	Center digital frequency	Power	HLCLMS gain	LCLMS gain
Jammer 1	22.5°	0.3	30 dB	-61.82 dB	-40.25 dB
Jammer 2	-18.1°	0.4	30 dB	-58.85 dB	-42.15 dB

$$p_i(n\Delta) = \frac{(n-1)p_i[(n-1)\Delta] + z_i^2(n\Delta)}{n},$$

for $i=1, 2, \dots, KL$. (32)

It should be noted that the beamforming algorithm described in (25) will be equivalent to (11) if the discrete cosine transform is used. This is due to the fact that the DCT matrix is an orthogonal matrix. However, this is not the case of (29) due to the normalized power in (31). Thus, the convergence property of (25) and (29) will differ dramatically.

In Ref. 10, the authors have shown that the hybrid LMS (HLMS) adaptive filtering algorithm performed more robust than the conventional LMS as well as the transformed domain NLMS adaptive algorithms. The fundamental concept behind the HLMS algorithm (described in Ref. 10) is to use the merits of the conventional LMS and the transformed domain NLMS adaptive algorithms to achieve the desired performance. The single channel hybrid LMS adaptive filtering algorithm discussed in Ref. 10 can be extended to the multiple channels adaptive array signal processing addressed in this paper. Similar to the approach of the hybrid adaptive filtering algorithm discussed in Ref. 10, the HLCLMS adaptive beamforming algorithm is the combination of the LCLMS adaptive beamforming algorithm and the normalized power version adaptive beamforming algorithm defined in (29). Thus, the weights updated equation of the HLCLMS beamforming algorithm can be expressed as

$$\mathbf{b}(n+1) = \mathbf{P}[\mathbf{b}(n) - \Lambda_s y(n)\mathbf{z}(n)] + \mathbf{a}, \quad (33)$$

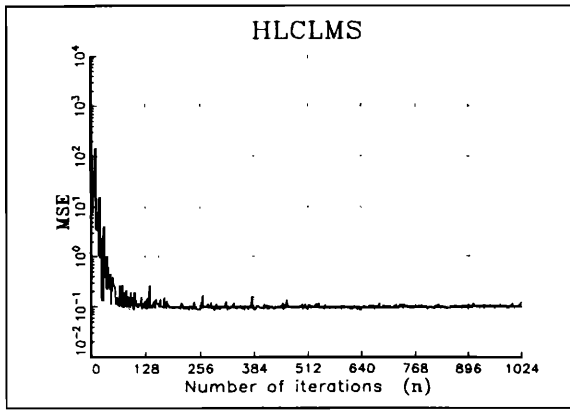
where

$$\Lambda_s = \begin{cases} \mu_1 \mathbf{I}, & \text{for initial adaptation process,} \\ \mu_2 \Lambda^{-1}, & \text{when input signals are sufficient.} \end{cases} \quad (34)$$

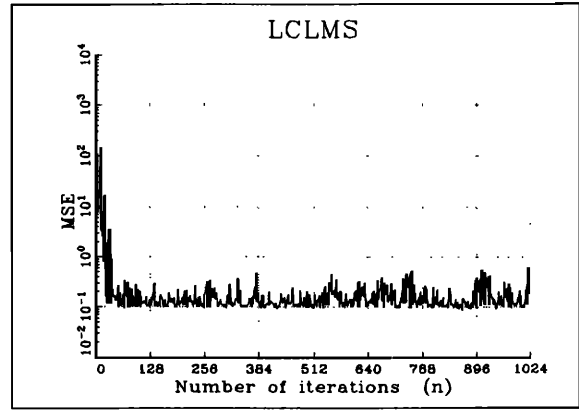
In (34), Λ^{-1} is the inverse matrix of Λ , and the diagonal matrix Λ is defined by

$$\Lambda = \text{diag}\{p_1(n\Delta), p_2(n\Delta), \dots, p_{KL}(n\Delta)\}. \quad (35)$$

Note that in (34), when $\Lambda_s = \mu_1 \mathbf{I}$, (33) can be viewed as the transformed domain expression of the Frost's LCLMS algorithm. As discussed earlier, this is due to the fact that the discrete cosine transform is an orthogonal matrix and the information is then preserved. Under this situation, the HLCLMS algorithm with $\Lambda_s = \mu_1 \mathbf{I}$ will perform equivalently to the Frost's LCLMS algorithm. This means that,

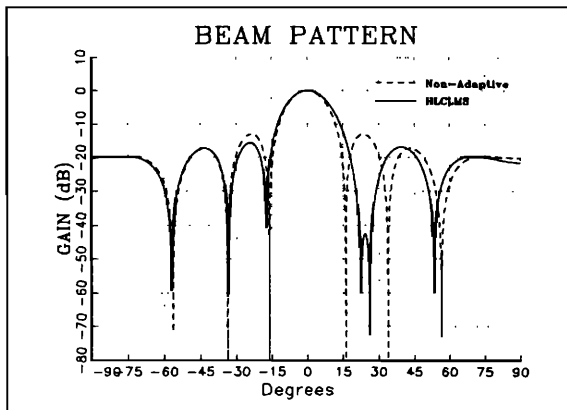


(a) HLCLMS

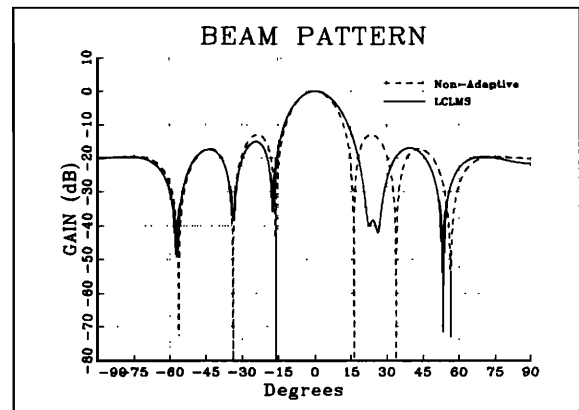


(b) LCLMS

FIG. 4. Learning curve of case 1.

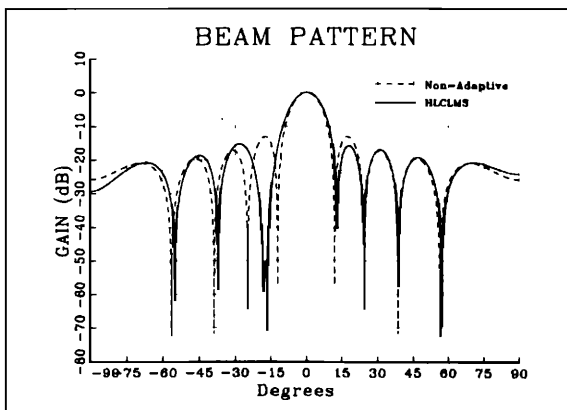


(a) HLCLMS

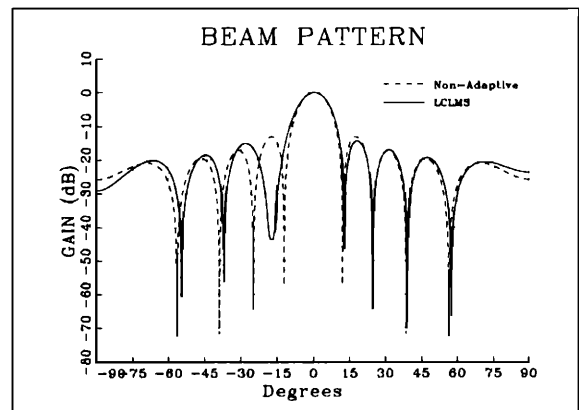


(b) LCLMS

FIG. 5. The beam pattern at digital frequency 0.3, jammer arrival angle is 22.5° (case 1).



(a) HLCLMS



(b) LCLMS

FIG. 6. The beam pattern at digital frequency 0.4, jammer arrival angle is -18.1° (case 1).

TABLE II. Case 2 jammers in simulation.

	Direction	Center digital frequency	Power	HLCLMS gain	LCLMS gain
Jammer 1	22.5°	0.3	40 dB	-65.15 dB	-42.25 dB
Jammer 2	-18.1°	0.4	20 dB	-52.44 dB	-31.25 dB

in the initial adaptation process, the HLCLMS algorithm is operating in the Frost's LCLMS algorithm mode. But, under this mode, the convergence rate of the HLCLMS algorithm will be affected by the power ratio between the input jammers. On the other hand, when Λ_s is setting to the value of $\mu_2 \Lambda^{-1}$, the HLCLMS algorithm will perform similar to the normalized power version algorithm defined in (29). That is, the convergence rate of the algorithm is less affected by the jammers' power ratio and we may say that the HLCLMS algorithm is operating in the normalized power version algorithm mode.

The directional pattern (that is, the relative sensitivity of response to signals for a specified frequency, ω_i , from various directions, θ) of the Frost's LCLMS structure can be easily shown to be

$$G(\theta) = \sum_{i=1}^K \sum_{m=1}^L \mathbf{w}_{(m-1)+} e^{-j\omega_i(m-1)} e^{(i-1)\omega_i \sin \theta}. \quad (36)$$

However, in the HLCLMS adaptive beamforming algorithm, the transformed weight vector \mathbf{b} is obtained instead of \mathbf{w} , thus (36) cannot be applied directly to obtain the directional pattern. In general, to compute the directional pattern we may take the inverse transform of the tap weights \mathbf{b} to obtain \mathbf{w} and then apply it into (36). This may result in an increase in the computation time if the beam pattern plots are required. For example, to calculate the 1024-point beam pattern at DECstation 2100 and measure the computation time, we found that the computation time will increase about 92.18% over the time spent using the LCLMS algorithm. To reduce the expense of computation time, we can simply derive the directional pattern in terms of the transformed weights (see Appendix B), so that the

computation time is increased only about 9.78% with respect to the one using (36).

III. SIMULATION RESULTS

In this section, the computer simulation is carried out to validate and investigate the performance of the presented method. We consider three performance metrics for two algorithms. The performance metrics are (1) the decibel (dB) interference rejection, (2) the improvement of convergence rates (ICR); and (3) the overall increment time (OIT). The algorithms are the LCLMS and HLCLMS adaptive beamforming algorithms. Both performance metrics ICR and OIT can be used to evaluate the overall performance improvement and will be discussed later.

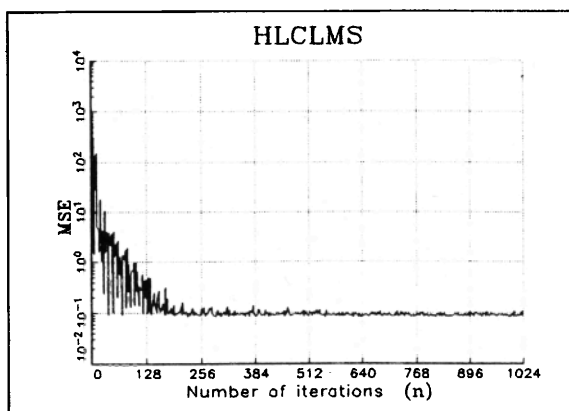
The received signal in each sensor consists of a broadband signal and two interferences (jammers) buried in a white Gaussian noise. For convenience, the desired look direction of the broadband signal is chosen to be $\theta=0^\circ$. The broadband signal is generated by sampling a pulse signal $(\alpha t)e^{-\alpha t}$ and then taking convolution with a time sequence generated by a random process. The Fourier transform of the pulse signal $(\alpha t)e^{-\alpha t}$ is given by

$$F(\Omega) = \text{FT}[(\alpha t)e^{-\alpha t}] = \frac{\alpha}{(\alpha + j\Omega)^2}, \quad (37)$$

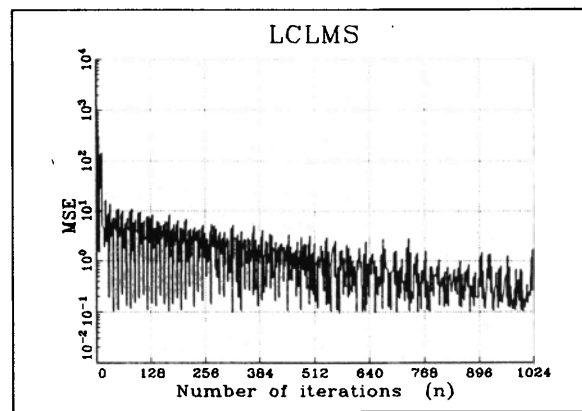
where $\text{FT}[\cdot]$ denote the Fourier transform and Ω is the analog radian frequency. The 3-dB bandwidth can be evaluated from (37) and the center frequency can be set anywhere by modulating the base-band spectrum. The directional interferences are two sinusoidal noise signals (jammers) incident at angles θ_1 and θ_2 , respectively.

If we use ζ to represent the underwater propagation speed of signal, the arrival of a given phase front at the reference sensor is earlier than at the next sensor by a number of time steps equal to

$$\kappa_i = \frac{d \sin \theta_i}{\zeta \Delta} = \frac{2\pi d \sin \theta_i}{\lambda \omega_i}, \quad (38)$$

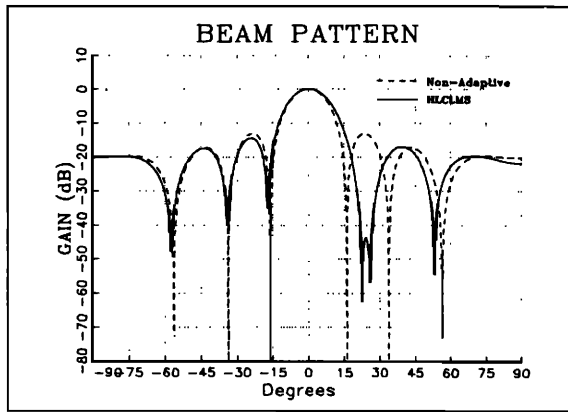


(a) HLCLMS

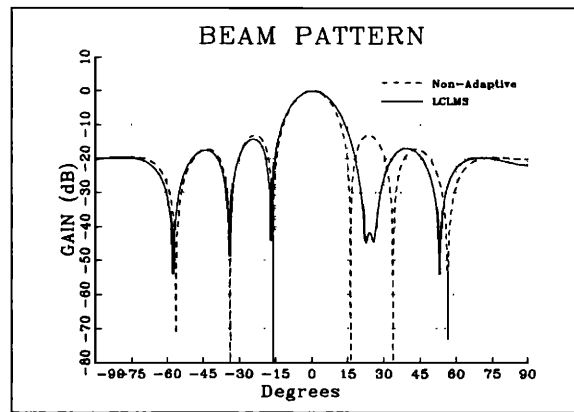


(b) LCLMS

FIG. 7. Learning curve of case 2.



(a) HLCLMS



(b) LCLMS

FIG. 8. The beam pattern at digital frequency 0.3, jammer arrival angle is 22.5° (case 2).

where Δ is the time step size (or sampling interval) in seconds, λ_i is the wavelength of signal with digital center radian frequency being ω_i ($\omega_i = \Omega_i \Delta$), and d is the distance of the sensor spaced apart. In our simulation, the power spectrum of the broadband signal is shown in Fig. 2. Here, $d = \lambda_0/2$, λ_0 is the wavelength at the radian frequency ω_0 , and ω_0 is the maximum digital radian frequency with a range $-\pi \leq \omega_0 \leq \pi$. So, for jammer 1,

$$\kappa_1 = \frac{2\pi(\lambda/2)\sin\theta_1}{\lambda_1\omega_1}$$

and for jammer 2,

$$\kappa_2 = \frac{2\pi(\lambda/2)\sin\theta_2}{\lambda_2\omega_2}$$

Therefore these two jammer signals impinging on the j th sensor are $x_j^1(n)$ and $x_j^2(n)$, for $j=1,2,\dots,K$, which are given by

$$x_j^1(n) = A_1 \cos\{[n + (j-1)\kappa_1]\omega_1\} \quad (39)$$

and

$$x_j^2(n) = A_2 \cos\{[n + (j-1)\kappa_2]\omega_2\}. \quad (40)$$

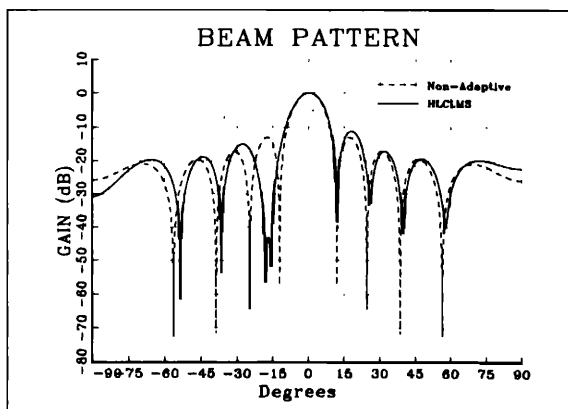
Thus each sensor has a broadband signal with two sinusoidal jammers buried in a white Gaussian noise, i.e.,

$$x_j(n) = s_j(n) + x_j^1(n) + x_j^2(n) + n_j(n). \quad (41)$$

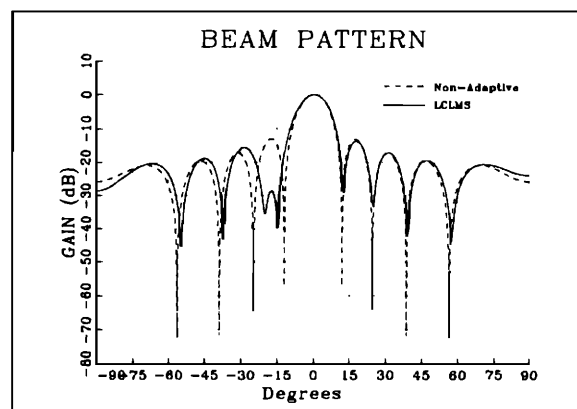
Let us define the jammers' power ratio (JPR) to be the ratio between the largest jammer power and the smallest jammer power. To study the effect of the JPR and the influence of the step size μ_s , some examples are given to illustrate the convergence property of the HLCLMS and LCLMS algorithms.

In the following computer simulations, the number of tap weights and the initial weight vector $\mathbf{w}(0)$ are fixed. Moreover, we assumed that the linear array has 12 sensors ($K=12$) on a line with each sensor having ten taps spaced at τ -second intervals (thus $KL=120$). The unit gain constraint has been put on the look direction. In all cases, the switch point used in the HLCLMS algorithm is set to 16.

The initial beam patterns are shown in each beam-pattern figure for digital frequencies at $f_1=0.3(=\omega_1/2\pi)$ and $f_2=0.4(=\omega_2/2\pi)$ corresponding to $\mathbf{w}(0)$. For instance, for $\Delta=1/1000$ (second), the corresponding analog frequencies of f_1 and f_2 will be 300 and 400 Hz, respectively. The direction of the jammers are placed on the side-



(a) HLCLMS



(b) LCLMS

FIG. 9. The beam pattern at digital frequency 0.4, jammer arrival angle is -18.1° (case 2).

TABLE III. Case 3 jammers in simulation.

	Direction	Center digital frequency	Power	HLCLMS gain	LCLMS gain
Jammer 1	22.5°	0.3	45 dB	-61.25 dB	-49.35 dB
Jammer 2	-18.1°	0.4	15 dB	-56.32 dB	-16.42 dB

lobe of the initial array pattern. Figure 3 depicts the signal and the jammers impinging on the linear array. For convenience, the angle of signal arrival is simple given as $\theta_s=0^\circ$. The signal bandwidth is 0.0461, the digital center frequency is 0.15, and the signal-to-noise ratio (SNR) is 0 dB. The angles of jammers arrival are θ_1 and θ_2 . To see the effect due to eigenvalue spread the following cases are considered.

A. Case 1

First, let us consider the case that the JPR being unity. The parameters and the results are listed in Table I. From Table I, we see that the jammer powers are 30 dB with respect to the target signal.

To make a fair comparison, the value of μ_1 is the same as the value of μ_s in LCLMS correspondingly. For the LCLMS algorithm to converge the step size (μ_s), from (12), should satisfy the following condition: $0 < \mu_s < 2.797 \times 10^{-6}$. In this case, the step size μ_s is chosen to be 1.4×10^{-6} . On the other hand, for the HLCLMS algorithm, the step sizes μ_1 and μ_2 are chosen to be 1.4×10^{-6} and 2.75×10^{-3} , respectively. The curves are obtained by averaging 500 independent trials. Figure 4(a) and (b) shows the learning curves of the HLCLMS and LCLMS algorithms. Observing Fig. 4 we found that the convergence rate of both algorithms is very similar, but the steady-state mean-squared error (MSE) of the HLCLMS algorithm has smaller variation compared with the LCLMS algorithm. Figures 5 and 6 are the corresponding frequency responses of the beam pattern of Fig. 4 at digital frequencies of 0.3 and 0.4. As can be seen from the responses of the beamformer, the nulls occur in the true

direction of the jammers. However, the use of the HLCLMS algorithm has at least an 15-dB attenuation over the LCLMS algorithm in the nulls direction.

B. Case 2

Next, if the JPR is increased to be 100 (the power difference of two jammers is 20 dB), and the step size μ_s (or μ_1) is bounded by $0 < \mu_s < 5.529 \times 10^{-7}$, the parameters and the results are given in Table II.

As can be seen from the learning curves shown in Fig. 7(a) and (b), the convergence speed of the HLCLMS algorithm is much faster than the convergence speed the LCLMS algorithm. Again, the beam patterns of the beamformer for a different frequency response are shown in Figs. 8 and 9. We can see that the use of the HLCLMS algorithm has at the least a 21-dB attenuation over the LCLMS algorithm in the nulls direction. Again, we concluded that the HLCLMS algorithm outperformed the LCLMS algorithm.

C. Case 3

Finally, in case 3, we consider the power ratio between two jammers to be 1000, and the step size μ_s (or μ_1) to be bounded by $0 < \mu_s < 1.764 \times 10^{-7}$. Again, from Table III, we found that the HLCLMS algorithm has deep nulls in the jammer directions. However, the LCLMS algorithm has a smaller null in the direction of jammer 2. In this case the attenuation of the nulls in the jammer directions using both the HLCLMS and the LCLMS algorithms is dramatically different as evident from Figs. 10-12.

In case 1, since the JPR is small, both of the HLCLMS and LCLMS adaptive beamforming algorithms have good convergence properties and depth nulls in the direction of the jammers. However, in case 2 and case 3, because the power ratio between the two jammers became relatively larger, the jammer with small power can be nulled deeper using the HLCLMS adaptive algorithm than the LCLMS adaptive algorithm. To see the transient property of the beam pattern, the three-dimensional chart for N from 0 to 90 iterations is shown in Fig. 13. In Fig. 13, the y axis indicates the iteration of adaptation processes. Here, only

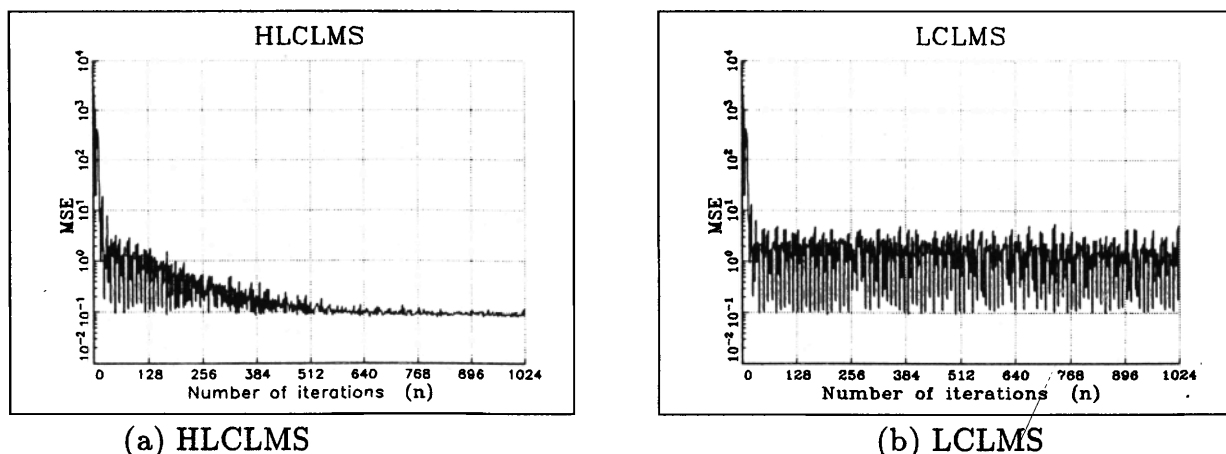
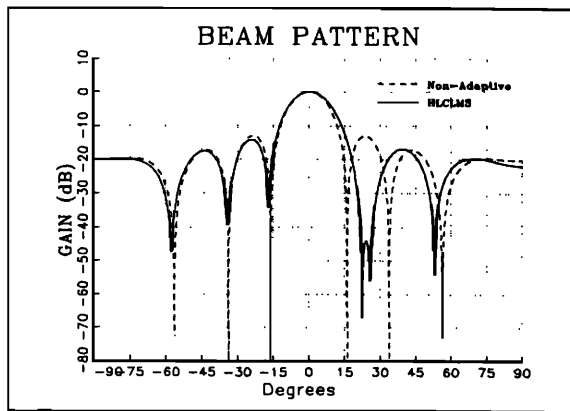
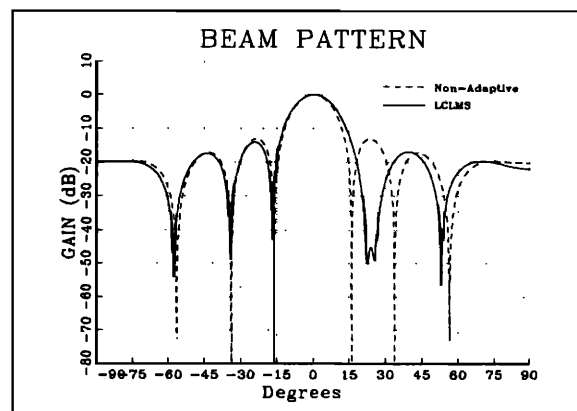


FIG. 10. Learning curve of case 3.



(a) HLCLMS



(b) LCLMS

FIG. 11. The beam pattern at digital frequency 0.3, jammer arrival angle is 22.5° (case 3).

the results of case 2 are given. From Fig. 13(a), we found that after 90 iterations, jammer 2 can be nulled about -25 dB but in Fig. 13(b) jammer 2 cannot be nulled satisfactorily. From the results just described, we concluded that the HLCLMS beamforming algorithm is more robust than the LCLMS beamforming algorithm.

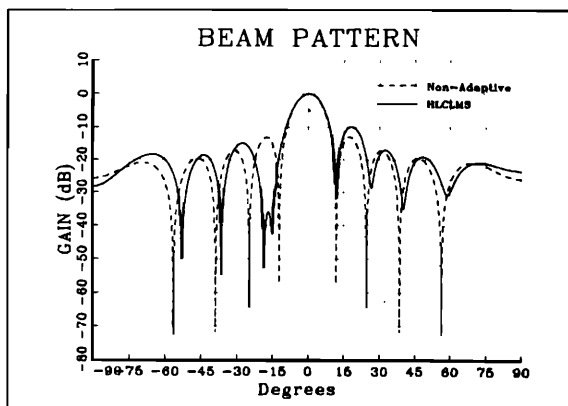
The overall performance improvement of the presented algorithm can be evaluated by the following two performance metrics, the *overall increment time* (OIT) and the convergence rate expressed in terms of the time constant. That is, when the *improvement of convergence rate* (ICR) is larger than the OIT the overall performance improvement can be achieved. This is because the ICR is the measurement of the improvement of the rate of convergence with respect to the Frost's LCLMS algorithm. The theoretical equations of the OIT and ICR can be derived under certain conditions but the details are neglected in this paper due to limited space. However, from the theoretical development we found that to satisfy the condition $ICR > OIT$, we should have $JPR > 1.959$. To be more specific, considering $JPR = 10$ as an example, the overall per-

formance can be evaluated by calculating the ICR and OIT. In this case, the overall computational requirement of the HLCLMS algorithm will be less than the LCLMS algorithm by 73.11%, when DEC station 2100 is employed.

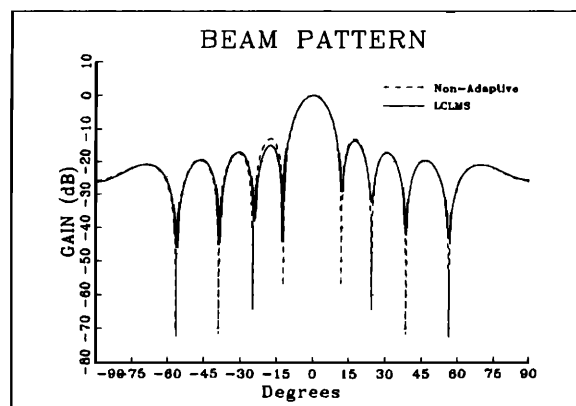
IV. CONCLUSIONS

In this paper, we have derived the HLCLMS adaptive beamforming algorithm in the discrete cosine transformed domain for multiple jammers suppression. As discussed in the last section, the Frost's LCLMS adaptive beamforming algorithm is very sensitive to the environment in which, the power ratio between jammers is relatively large. To overcome this problem, we applied the hybrid LMS adaptive filtering technique to Frost's adaptive beamformer.

From the simulation results, the advantage of using the HLCLMS adaptive beamforming algorithm has been demonstrated. In all cases, we have shown that the HLCLMS beamforming algorithm has a faster convergence rate and smaller steady-state MSE than the LCLMS beamforming algorithm. Moreover, in case 1, since the



(a) HLCLMS



(b) LCLMS

FIG. 12. The beam pattern at digital frequency 0.4, jammer arrival angle is -18.1° (case 3).

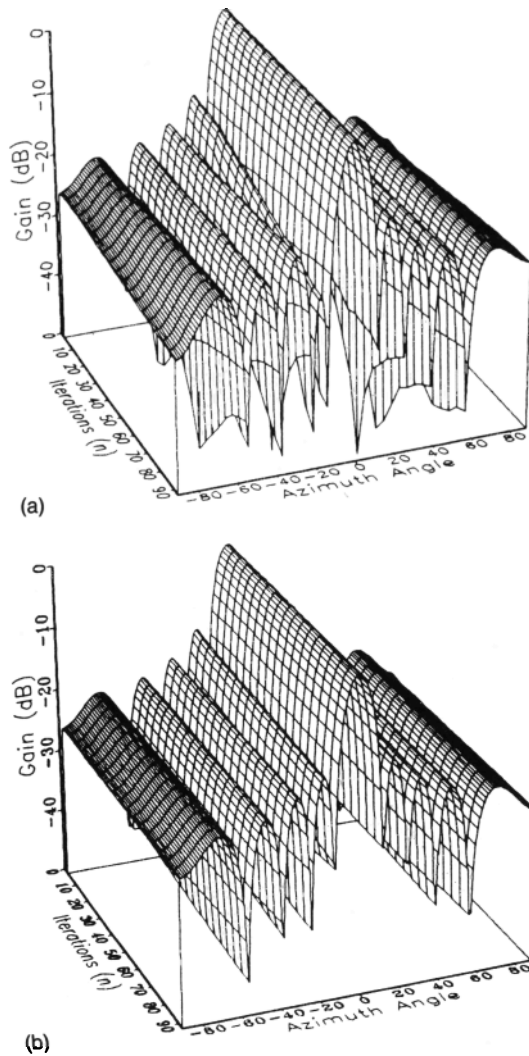


FIG. 13. (a) The 3-D beam pattern of HLCLMS, digital frequency 0.4 (case 2); (b) 3-D beam pattern of LCLMS, digital frequency 0.4 (case 2).

JPR is small in both cases, both the HLCLMS and LCLMS adaptive beamforming algorithms have good convergence properties and depth nulls in the direction of jammers. However, in case 2 and case 3, because the power ratio between two jammers became relatively larger, the jammer with small power can be nulled deeper using the HLCLMS adaptive algorithm than the LCLMS adaptive algorithm. The attenuation of the nulls in the jammer di-

rections by the HLCLMS algorithm has remained in the range of 50–60 dB in all the cases. This is not the case when the conventional Frost's beamforming algorithm is used. Moreover, the overall performance improvement can be achieved if the condition $JPR > 1.959$ is satisfied.

APPENDIX A

In this Appendix, we would like to show that

$$\mathbf{P} = \Psi^T \mathbf{P} \Psi$$

with

$$\mathbf{P} = \mathbf{I} - \mathbf{C}(\mathbf{C}^T \mathbf{C})^{-1} \mathbf{C}^T$$

and Ψ^T as defined in (19). By definition, the constraint matrix \mathbf{C} can be rewritten as

$$\mathbf{C} = [\mathbf{c}_1, \dots, \mathbf{c}_j, \dots, \mathbf{c}_L] = \begin{bmatrix} \mathbf{1}_K & \mathbf{0}_K & \mathbf{0}_K & \cdots & \mathbf{0}_K \\ \mathbf{0}_K & \mathbf{1}_K & \mathbf{0}_K & \cdots & \mathbf{0}_K \\ \vdots & \vdots & \vdots & \ddots & \vdots \\ \mathbf{0}_K & \cdots & \mathbf{0}_K & \mathbf{1}_K & \mathbf{0}_K \\ \mathbf{0}_K & \cdots & \mathbf{0}_K & \mathbf{0}_K & \mathbf{1}_K \end{bmatrix}_{KL \times L} \quad (\text{A1})$$

Consequently,

$$\mathbf{C}(\mathbf{C}^T \mathbf{C})^{-1} \mathbf{C}^T = \begin{bmatrix} \mathbf{A}_K & \mathbf{0}_K & \cdots & \mathbf{0}_K \\ \mathbf{0}_K & \mathbf{A}_K & \cdots & \mathbf{0}_K \\ \vdots & \vdots & \ddots & \vdots \\ \mathbf{0}_K & \mathbf{0}_K & \cdots & \mathbf{A}_K \end{bmatrix}_{KL \times KL}, \quad (\text{A2})$$

where

$$\mathbf{A}_K = [\mathbf{1}_K (\mathbf{1}_K^T \mathbf{1}_K)^{-1} \mathbf{1}_K^T] \quad (\text{A3})$$

and $\mathbf{0}_K$ is the zero matrix. To prove $\mathbf{P} = \Psi^T \mathbf{P} \Psi$, we first show that

$$\Psi^T \mathbf{C}(\mathbf{C}^T \mathbf{C})^{-1} \mathbf{C}^T \Psi = \mathbf{C}(\mathbf{C}^T \mathbf{C})^{-1} \mathbf{C}^T. \quad (\text{A4})$$

Substituting (17), (A2), and (A3) into (A4), we have

$$\Psi^T \mathbf{C}(\mathbf{C}^T \mathbf{C})^{-1} \mathbf{C}^T \Psi = \begin{bmatrix} \sum_{m=0}^{L-1} \phi_{0m} \phi_{0m} \mathbf{A}_K & \sum_{m=0}^{L-1} \phi_{0m} \phi_{1m} \mathbf{A}_K & \cdots & \sum_{m=0}^{L-1} \phi_{0m} \phi_{(L-1)m} \mathbf{A}_K \\ \sum_{m=0}^{L-1} \phi_{1m} \phi_{0m} \mathbf{A}_K & \sum_{m=0}^{L-1} \phi_{1m} \phi_{1m} \mathbf{A}_K & \cdots & \sum_{m=0}^{L-1} \phi_{1m} \phi_{(L-1)m} \mathbf{A}_K \\ \vdots & \vdots & \ddots & \vdots \\ \sum_{m=0}^{L-1} \phi_{(L-1)m} \phi_{0m} \mathbf{A}_K & \sum_{m=0}^{L-1} \phi_{(L-1)m} \phi_{1m} \mathbf{A}_K & \cdots & \sum_{m=0}^{L-1} \phi_{(L-1)m} \phi_{(L-1)m} \mathbf{A}_K \end{bmatrix}. \quad (\text{A5})$$

Due to the orthonormal property described in (16), (A5) can be simplified as

$$\begin{aligned} \Psi^T C (C^T C)^{-1} C^T \Psi &= \begin{bmatrix} \mathbf{A}_K & \mathbf{0}_K & \cdots & \mathbf{0}_K \\ \mathbf{0}_K & \mathbf{A}_K & \cdots & \mathbf{0}_K \\ \vdots & \vdots & \ddots & \vdots \\ \mathbf{0}_K & \mathbf{0}_K & \cdots & \mathbf{A}_K \end{bmatrix}_{KL \times KL} \\ &= C (C^T C)^{-1} C^T. \end{aligned} \quad (\text{A6})$$

Using the result of (A6), we can readily prove that

$$\begin{aligned} \Psi^T \mathbf{P} \Psi &= \Psi^T [\mathbf{I} - C (C^T C)^{-1} C^T] \Psi \\ &= \mathbf{I} - \Psi^T [C (C^T C)^{-1} C^T] \Psi \\ &= \mathbf{I} - C (C^T C)^{-1} C^T = \mathbf{P}. \end{aligned}$$

APPENDIX B

In this Appendix, the directional pattern, in terms of the transformed weights, is derived. To do that, we recalled from (36), the beam pattern gain formula of the conventional Frost's LCLMS structure was given by

$$G(\theta) = \sum_{i=1}^K \sum_{m=1}^L \mathbf{w}_{(m-1)+i} e^{-j\omega_i(m-1)} e^{(i-1)\omega_i \sin \theta}, \quad (\text{B1})$$

where ω_i is the test frequency. Now, if we define \mathbf{q} and \mathbf{w}_i as

$$\mathbf{q} = [1, e^{-j\omega_i}, e^{-j2\omega_i}, \dots, e^{-j(L-1)\omega_i}]^T \quad (\text{B2})$$

and

$$\mathbf{w}_i = [w_i, w_{K+i}, w_{2K+i}, \dots, w_{(L-1)K+i}]^T, \quad (\text{B3})$$

respectively, then (B1) can be rewritten as

$$G(\theta) = \sum_{i=1}^K \mathbf{w}_i^T \mathbf{q} e^{(i-1)\omega_i \sin \theta}. \quad (\text{B4})$$

Recalled from (23) we have

$$\mathbf{b} = \Psi^T \mathbf{w}, \quad (\text{B5})$$

for convenience, we also define \mathbf{b}_i , the corresponding transformed weight vector of \mathbf{w}_i , as

$$\mathbf{b}_i = [b_i, b_{K+i}, b_{2K+i}, \dots, b_{(L-1)K+i}]^T. \quad (\text{B6})$$

Accordingly, (B5) can be rearranged as

$$\mathbf{b}_i = \phi^T \mathbf{w}_i \quad (\text{B7})$$

or

$$\mathbf{w}_i^T = \mathbf{b}_i^T \phi^T, \quad i=1, 2, \dots, K. \quad (\text{B8})$$

To simplify the beam pattern gain formula, we substitute (B8) into (B4),

$$G(\theta) = \sum_{i=1}^K \mathbf{b}_i^T \phi^T \mathbf{q} e^{(i-1)\omega_i \sin \theta}. \quad (\text{B9})$$

Moreover, we define

$$\mathbf{q}' = \phi^T \mathbf{q} \quad (\text{B10})$$

then (B9) will become

$$G(\theta) = \sum_{i=1}^K \mathbf{b}_i^T \mathbf{q}' e^{(i-1)\omega_i \sin \theta}. \quad (\text{B11})$$

Since, from (B10), the parameter \mathbf{q}' can be pre-calculated, to implement (B11) only one DCT with length L is required.

¹L. C. Codara, "Improved LMS Algorithm for Adaptive Beamforming," IEEE Trans. Antennas Propag. 38(10), 1631-1635 (1990).

²S. M. Yuen, "Exact Least-Squares Adaptive Beamforming Using an Orthogonalization Network," IEEE Trans. Aero. Elec. System 27(2), 311-330 (1991).

³J. Capon, R. J. Greenfield, and J. Kolker, "Multidimensional Maximum-Likelihood Processing of a Large Aperture Seismic Array," Proc. IEEE 55(2), 192-211 (1967).

⁴L. J. Griffiths and J. W. Jim, "An Alternative Approach to Linearly Constrained Adaptive Beamforming," IEEE Trans. Antennas Propag. 30, 27-34 (1982).

⁵O. L. Frost, III, "An Algorithm for Linearly Constraint Adaptive Array Processing," Proc. IEEE 60(8), 926-935 (1972).

⁶O. L. Frost, III, "Adaptive Least Squares Optimization Subject to Linear Equality Constraints," Stanford Electron. Lab., Stanford, CA, Doc.

⁷I. J. Good and K. Koog, "A Paradox Concerning Rate of Information," Inform. Control 1, 113-116 (1958). SEL-70-055, Tech. Rep. TR 6796-2 (1970).

⁸N. Ahmed, T. Natarajan, and K. R. Rao, "Discrete Cosine Transform," IEEE Trans. Comput. 23, 90-93 (1974).

⁹S. J. Chern, "Recursive Discrete Cosine Transform and Discrete Sine Transform," Proc. of 1987 Telecom. Symposium, Taiwan, R.O.C., 307-314 (1987).

¹⁰S. J. Chern and B. Y. Chen, "The Study of Hybrid Adaptive Least Mean Square (LMS) Filtering Algorithm With Variable Step-size," Proc. Natl. Sci. Council, R.O.C. Pt. A 13(3), 124-130 (1989).